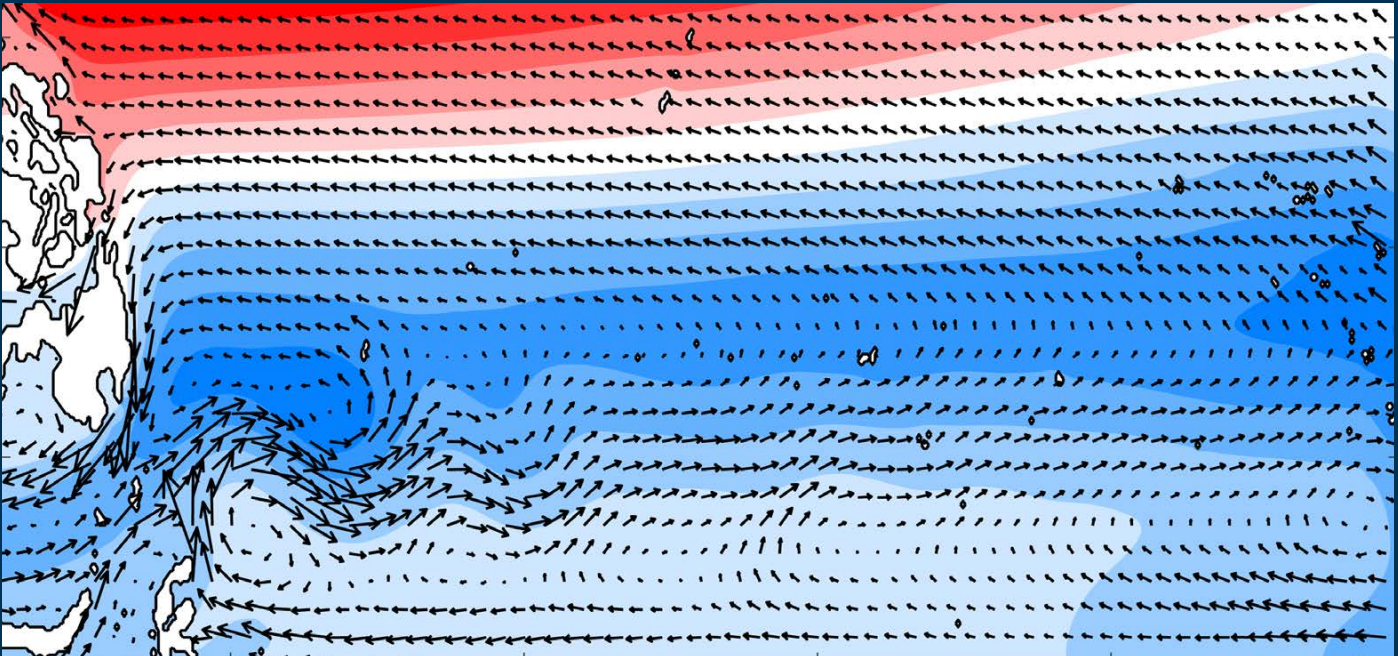


# PALAU'S EFFECTS ON REGIONAL-SCALE OCEAN CIRCULATION

By Ganesh Gopalakrishnan and Bruce D. Cornuelle



**ABSTRACT.** The Republic of Palau, a group of islands in the western tropical Pacific Ocean, is located between the westward-flowing North Equatorial Current (NEC) to the north and the eastward-flowing North Equatorial Countercurrent (NECC) to the south, and the Mindanao Eddy (ME) lies to the west. This unique geographical location may make Palau an oceanographically sensitive region due to strong equatorial zonal flows encountering steep island topography. We investigate the effect Palau has on the regional ocean circulation through numerical model simulations with identical forcing but differing bathymetry: one with Palau and the other without it. The simulations use realistic initial conditions—monthly climatological atmospheric forcing, open-ocean boundary conditions, and runoff fluxes—and were run for up to 37 years to distinguish between model intrinsic variability and deterministic differences. The significant differences between the two solutions show that Palau's effect on circulation is localized and small. The model state differences, quantified as percentage of model variability near Palau from the 37-year solution, are about 20% for sea surface height, 25% for surface velocities, and <1% for surface temperature and salinity. The subsurface velocity fields around Palau show a two-layered flow, as previously reported by other authors, with upper layer flow from the surface to 300 m, and a lower layer flow from 300 m to 3,000 m. The topographic form stress on Palau is <10% of the vertically integrated total form stress in the 5°N–10°N latitudinal band, and when the island is removed from model simulations, the stress is redistributed within the region. Although these results are restricted to model resolution scales and physics, they provide an estimate of the influence of Palau on the large-scale northwestern tropical Pacific Ocean circulation.

**IN PLAIN WORDS.** The Republic of Palau is of considerable oceanographic interest due to its unique geographical location sandwiched between strong equatorial currents. We investigate the effect of Palau's steep subsurface topography on regional circulation through long-term ocean model simulations that use identical climatological forcings but with and without the Palau island and ridge. The differences between the model solutions showed that Palau's effect on regional circulation is localized and small. This impact can be quantified by calculating the force that the main island exerts on the flow and how that changes when the island is removed. These results are obtained at a relatively coarse model resolution and with physical compromises, and so gives a lower bound on Palau's effects on large-scale northwestern tropical Pacific Ocean circulation.

## INTRODUCTION

The mean circulation in the northwestern tropical Pacific Ocean consists of the broad, wind-driven, westward-flowing North Equatorial Current (NEC); the relatively weak and shallow eastward-flowing, surface North Pacific Subtropical Countercurrent (STCC) at 18°N–25°N (Qiu and Chen, 2010); the eastward-flowing North Equatorial Countercurrent (NECC); and two western boundary currents, the Kuroshio Current (KC) that flows northward to the east of Taiwan and the southward-flowing Mindanao Current (MC; Nitani, 1972). The NEC bifurcates near the Philippine coast into the KC and MC (Nitani, 1972; Qu et al., 1998), and is strongly influenced by wind stress curl through Sverdrup dynamics (Qu and Lukas, 2003).

The Republic of Palau is located near the center of the Mindanao Dome (MD; Kashino et al., 2011), an area of upper ocean cyclonic circulation forced by seasonal positive wind stress curl that lies between the NEC to the north and the retroflecting NECC to the south, and on the east edge of the Mindanao Eddy (ME; Kashino et al., 2011). Even though Palau is a small island group in the western tropical Pacific, its unique location

sandwiched between two major circulation gyres has made it a region of considerable interest to oceanographers.

For orientation, **Figure 1** shows the mean sea surface height (SSH) and surface currents from a long-term model solution using climatological forcings. The details of the ocean model are discussed in the next section. **Figure 1a** and a zoomed version for Palau (**Figure 1b**) show the westward-flowing NEC bifurcating around 12°N into the northward-flowing KC along the coast of Taiwan and the southward-flowing MC along the Philippine coast. A part of the MC flows westward and contributes to the Indonesian Throughflow (ITF), while the other part reenters the tropical Pacific and merges with the NECC flowing eastward. A quasi-stationary anticyclonic eddy known as Halmahera Eddy (HE) is observed northeast of Halmahera island. The HE, a recirculation of the NECC, promotes mixing of waters from the Northern and Southern Hemispheres and contributes to the ITF (Kashino et al., 2013). A cyclonic eddy known as the Mindanao Eddy (ME) is observed west of Palau. The ME, a recirculation of the MC, is more of an intermittent feature (Kashino et al., 2013;

Schönau and Rudnick, 2017), making it less important compared to other major circulation features such as NEC, NECC, and HE. The nearby MD is generated in late fall due to local upwelling forced by positive wind stress curl associated with the northeast Asian winter monsoon (Masumoto and Yamagata, 1991; Kashino et al., 2011). The MD expands eastward with a recirculation that includes the westward-flowing NEC to the north, the southward-flowing MC to the west, and the eastward-flowing NECC to the south. Taken together, the MD, MC, ME, HE, NEC, and NECC comprise a complex circulation pattern around Palau. The motivation for the experiment reported here is to assess the effect of Palau on these features in order to see whether their positions with respect to Palau are coincidence or dynamically driven.

It would also be interesting to understand how the presence of Palau influences regional ocean circulation features including: (1) the two-layered flow around Palau, (2) the NEC, the North Equatorial Undercurrent (NEUC; Qiu et al., 2013), and the NECC at its northern and southern edges, (3) the stability of the MD with respect to seasonal positive wind stress curl, and (4) the gener-

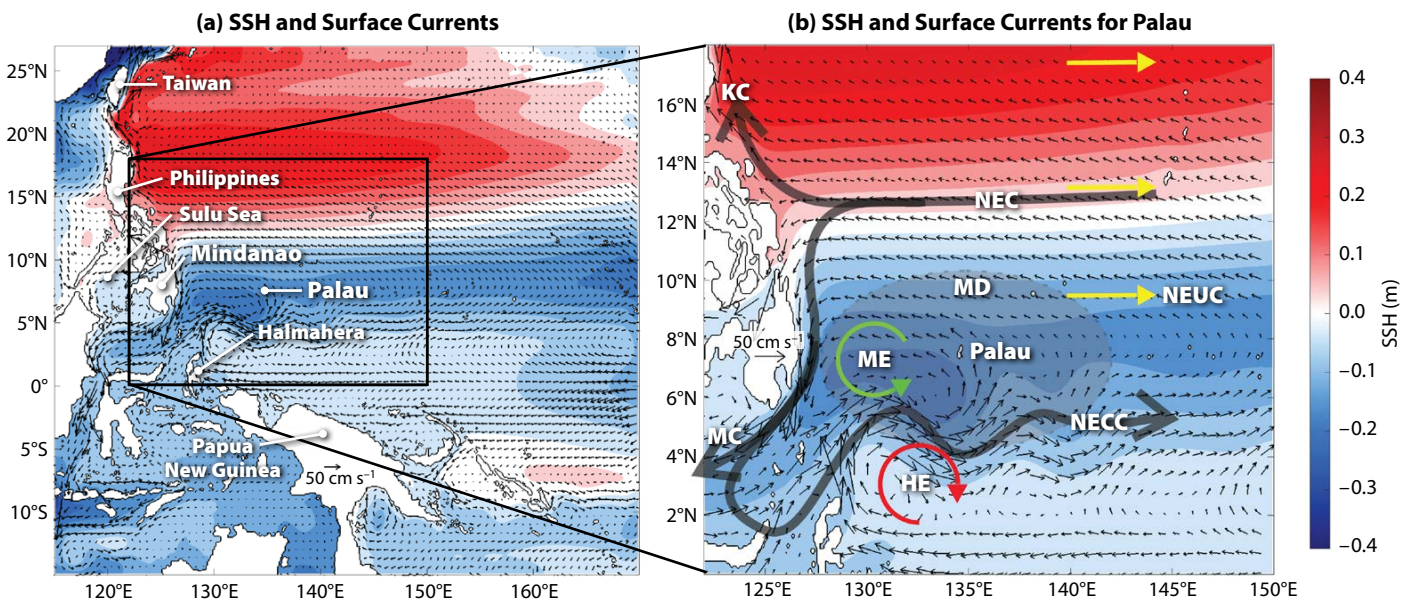


**FIGURE 1.** Model mean sea surface height (SSH) and surface velocities from the 37-year climatological run with Palau included (CTL). (a) Model solutions are shown for the whole domain. (b) A zoomed version of flow around Palau includes arrows that track major flow features. The shading provides SSH values in meters. KC = Kuroshio Current. NEC = North Equatorial Current. MD = Mindanao Dome. NEUC = North Equatorial Undercurrent. ME = Mindanao Eddy. NECC = North Equatorial Countercurrent. MC = Mindanao Current. HE = Halmahera Eddy.

ation of local western boundary currents by the blocking of the NEC, similar to the origin of KC and MC western boundary currents where the NEC reaches the Philippine coast. Because wind forcing plays an important role in western tropical Pacific Ocean circulation, it is interesting to understand how the presence of the island affects the wind-driven flow and the momentum transfer from the ocean into the steep island topography. Because the Palau islands do not have strong relief, we are not considering the impact of the islands on the wind field.

Using ocean general circulation model (OGCM) simulations with and without Palau, this study examines the effect of Palau on the regional circulation. Karnauskas et al. (2007) used these kinds of bathymetry perturbation experiments to understand the effect of the Galápagos islands on the equatorial Pacific cold tongue using a reduced-gravity OGCM. Another study using a similar methodology was reported by Wang et al. (2016), where Massachusetts Institute of Technology general circulation model (MITgcm; Marshall et al., 1997) simulations were used to study the effect of the Kerguelen Plateau on Southern Ocean circulation. Note that the Galápagos islands and the Kerguelen Plateau are relatively large topographic features when com-

pared to Palau. Here, we implement a similar approach in a regional model of the northwestern tropical Pacific using the MITgcm to examine the effect of Palau on regional ocean circulation. To find statistically significant differences, the simulations used climatological atmospheric forcing, open-ocean boundary conditions, and runoff fluxes, and were run for up to 37 years. The model state differences, including topographic form stress, were calculated between the two simulations. Analysis of these calculations revealed that the island contributes only locally to modifications of topographic form stress and ocean state and does not contribute to the large-scale global circulation gyres such as NEC and NECC.

This work is part of the Office of Naval Research's (ONR) Departmental Research Initiative (DRI): Flow Encountering Abrupt Topography (FLEAT). Other observational and modeling studies reported in this *Oceanography* FLEAT special issue focus on the fine-scale and time-dependent circulation features around Palau and other adjacent island groups. In contrast, this study aims to understand modifications to large-scale circulation features that occur when currents encounter the steep topographic features of Palau.

The next section describes our meth-

odology using the numerical ocean model. It is followed by a section that explains our topography perturbation experiments with and without Palau as well as long-term climatological simulations. Results of the numerical experiments are discussed next and are followed by a summary and a discussion.

## OCEAN MODEL

The MITgcm is based on the primitive (Navier-Stokes) equations for a sphere under the Boussinesq approximation. The model vertical grid follows  $z$ -coordinates, and the equations are discretized using the third-order direct-space-time advection scheme in a staggered Arakawa C-grid. The model has been widely used in numerous state estimations and predictions, and in adjoint sensitivity studies at global and regional scales (e.g., Stammer et al., 2002; Fukumori et al., 2004; Menemenlis et al., 2005; Hoteit et al., 2009, 2010; Kohl et al., 2007; Mazloff et al., 2010; Zhang et al., 2012; Gopalakrishnan et al., 2013a,b). It has also been used in various theoretical and idealized model studies as well as in realistic regional-scale oceanic process studies (e.g., Legg et al., 2006; Gopalakrishnan et al., 2013c; Edwards et al., 2004a,b; Kim et al., 2015; Musgrave and Peacock, 2016).

The MITgcm model implementation we used here was also used in the ONR DRI: Origins of the Kuroshio and Mindanao Currents (OKMC; Qiu et al., 2015; Schönau et al., 2015; Lien et al., 2015). It was used for model simulations and to make Western Pacific Ocean State Estimates (WPOSE) and forecasts ([http://ecco.ucsd.edu/nwpac\\_results1.html](http://ecco.ucsd.edu/nwpac_results1.html)). WPOSE is also analyzed in the studies reported in this special issue (Schönau et al., 2019, and Schramek et al., 2019). The model is used here as a tool to explore the effect of Palau on regional circulation using topographic perturbation experiments. The details of the model setup and forcings are summarized in **Tables 1 and 2**, respectively.

The model is integrated from 2009

TABLE 1. MITgcm-WPOSE Model Description

DESCRIPTION	VALUE/SOURCE
Longitude	115°E–170°E
Latitude	15°S–27°N
Topography	NRL DBDB2 global 2-minute topography (NRL-DBDB2v2.0), with maximum depth of 6,500 m
Horizontal grid	1/12° × 1/12° (~9 km) spherical polar grid
Vertical grid	50 vertical $z$ -levels, with level spacing gradually increasing with depth from 2.5 m at the surface to a maximum of 300 m near the bottom
Subgrid-scale parameterization	Vertical, second-order diffusive operator
Vertical diffusivity and viscosity parameterization	K-profile parameterization (KPP; Large et al., 1994) with a background value of $2 \times 10^{-5} \text{ m}^2 \text{ s}^{-1}$
Horizontal diffusivity and viscosity (second order)	$1 \times 10^2 \text{ m}^2 \text{ s}^{-1}$
Horizontal diffusivity and viscosity (fourth order)	$1 \times 10^{11} \text{ m}^4 \text{ s}^{-1}$

through 2014 using initial conditions and open-ocean boundary conditions from the Hybrid Coordinate Ocean Model (HYCOM; Chassignet et al., 2007) global 1/12° daily analysis (<http://hycom.org/dataserver/glb-analysis>); HYCOM includes Navy Coupled Ocean Data Assimilation (NCODA; Cummings, 2005), ERA-Interim atmospheric forcing produced by the European Centre for Medium Range Weather Forecasts (Dee et al., 2011), and annual climatology of continental runoff (Fekete et al., 2002). Comparison (not shown) of this unconstrained model solution with satellite-derived SSH and sea surface temperature (SST) suggested that the model is capable of simulating regional ocean circulation with comparable means and variability for the equatorial (NEC, NECC) and western boundary (KC, MC) currents.

## MODEL EXPERIMENTS WITH/WITHOUT PALAU

We performed two simulations using model setups that differed only in the bathymetry around Palau. The con-

trol model (CTL) bathymetry, which includes Palau, is as described in Table 1 (NRL-DBDB2-v2.0). The perturbed experiment (NoP) used modified bathymetry with a plain replacing Palau: the ocean floor was set to 3,000 m for all grid cells within the 3,000 m contour around Palau. Figure 2a shows CTL

bathymetry near Palau, and Figure 2b shows the NoP bathymetry for the same region. Figure 2c shows the bathymetry changes (CTL–NoP).

These long-term simulations were initialized from HYCOM/NCODA analysis on January 1, 2012, and used monthly climatological ERA-Interim atmospheric

TABLE 2. MITgcm-WPOSE Model Forcings

DESCRIPTION	SOURCE
Initial conditions	The Hybrid Coordinate Ocean Model (HYCOM; Chassignet et al., 2007) global 1/12° daily analysis ( <a href="http://hycom.org/dataserver/glb-analysis">http://hycom.org/dataserver/glb-analysis</a> ) using Navy Coupled Ocean Data Assimilation (NCODA; Cummings, 2005)
Open-ocean boundary (OB) conditions	HYCOM/NCODA global 1/12° estimates of temperature, salinity, and horizontal velocities, sampled every seven days.
OB sponge layer	Buffer zone of 1.5°, with restoring timescales varying linearly from one day at the boundary to five days at the inner edges of the sponge layers. HYCOM/NCODA normal velocity fields across the OB have been adjusted to have zero net volume flux into the model domain.
Atmospheric forcing	ECMWF ERA-Interim (Dee et al., 2011).
Atmospheric state	Bulk formulation (Large and Pond, 1981) for the computation of the atmospheric fluxes. The atmospheric forcing includes air temperature, specific humidity, zonal and meridional wind speed at 10 m from the ground, total precipitation, and short and long wave radiative fluxes, sampled every six hours on an 80 km horizontal resolution.
Runoff fluxes	Annual climatology of continental runoff (Fekete et al., 2002).

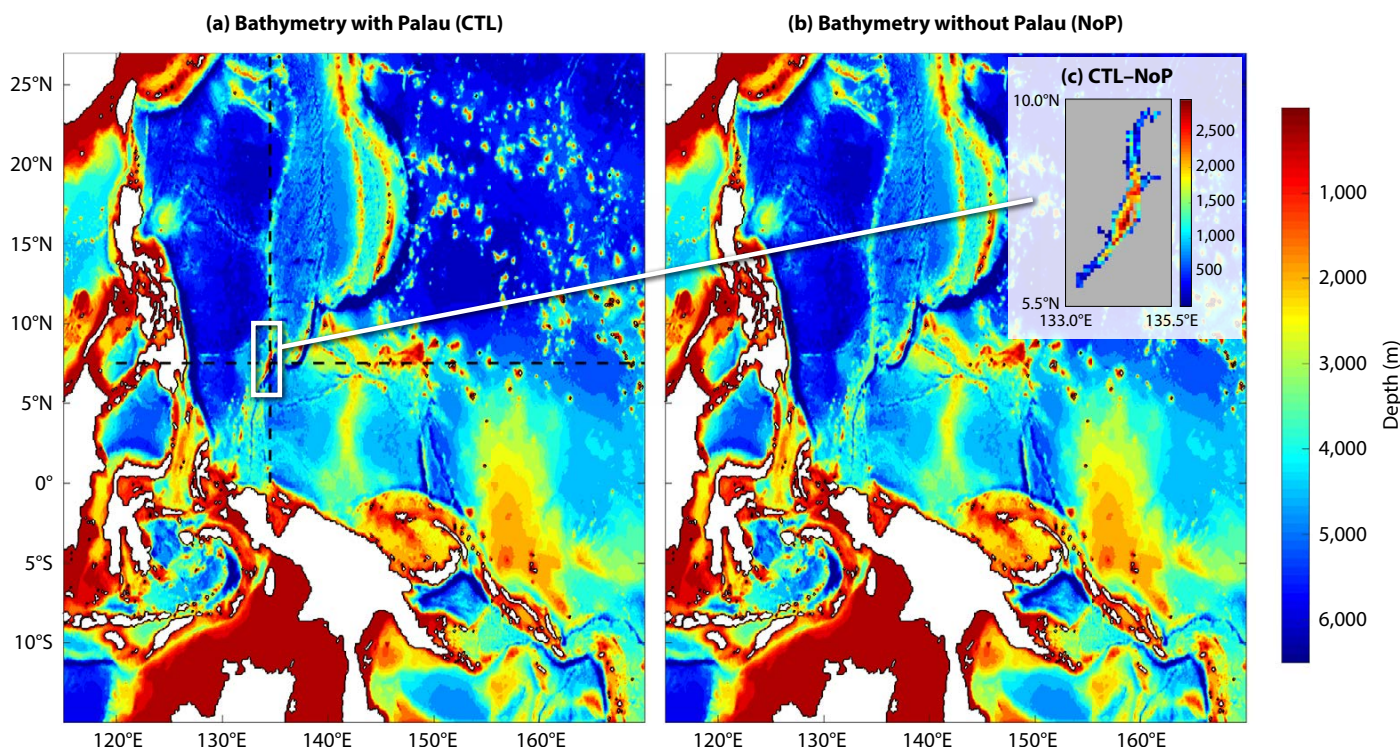


FIGURE 2. Model bathymetry (a) with Palau (CTL) and (b) without Palau (NoP). (c) The difference in depths (CTL–NoP). The area of (c) is marked by the white box in (a). The black dashed lines in (a) mark the sections shown in Figure 3.

forcing, HYCOM/NCODA open-ocean boundary conditions, and runoff fluxes. The simulations were as long as was practical in order to average down the intrinsic (e.g., eddy) variability and to focus on statistically significant differences in the circulation features with and without Palau. Simulations were run for 37 years, and the differences and statistics, sampled at 10, 25, and 37 years, showed little change at the end.

## RESULTS

### Modifications to the Regional Ocean Circulation

Figure 3a,b shows the SSH differences through time between the two simulations (NoP-CTL) along latitude and longitude lines centered on Palau: 120°E–170°E at 7.5°N, and 0°N–27°N at 134.55°E, respectively (longitudinal and latitudinal sections are marked by dashed black lines in Figure 2a). Although the model bathymetry is changed only at Palau, the solution changes everywhere in the model, which we hypothesize is primarily due to the model intrinsic variability such as eddy interactions and instabilities. At 7.5°N, the SSH differences are visible immediately to the west of Palau, and they reach apparent equilib-

rium near Palau after a year with a range of  $\pm 5$  cm. Although the growth is slower to the east, the differences remain small at the eastern boundary because of the restoring to the outer model (open-ocean boundary conditions).

The SSH differences along the section at 134.55°E cover three regions of large-scale flows: the NECC, the NEC, and the STCC in the area from 18°N to 25°N. The SSH differences in this section again appear quickly at Palau, with values in the range  $\pm 5$  cm, and fill in much more rapidly to the south than to the north, which does not come into equilibrium until after about three years. The SSH differences in the NEC region between 9°N and 18°N are almost zero, which is expected because this region exhibits very low SSH variability in both the model and observations (Qiu, 1999; Ducet et al., 2000). The SSH differences in the eddy-active STCC region from 18°N to 25°N range within  $\pm 10$  cm and only reach equilibrium after more than two years from the start of the simulation, which sets a timescale for the influence of perturbations near Palau to reach the STCC. The SSH differences at the northern boundary are almost zero, again due to the boundary restoring.

Figure 4a shows a plan view of mean

SSH differences (NoP-CTL). The mean differences for 10-, 25-, and 37-year integration are similar near Palau, but decrease in most other areas as integration time increases. Only differences that were larger than three times the standard error (SE) of the mean difference were considered significant and are crosshatched (with black) in the figure. The SE is defined as

$$\sigma_{\bar{x}} = \frac{\sigma}{\sqrt{n}},$$

where  $n$  is the number of independent samples (model solutions were sampled as monthly means over the 37-year simulation period) and  $\sigma$  is the standard deviation. The statistically significant regions are mostly near Palau, and even relatively large differences in the STCC are generally not statistically significant.

The mean SSH differences are positive (negative) to the north (south) of Palau but are only significant on the north end due to the smaller variability of the NEC compared to the NECC. The mean SSH difference range is  $\pm 1$  cm, about 20% of the size of the spatial variation of the SSH near Palau (5 cm). The positive difference in the north is consistent with Palau acting as a barrier for the NEC and increasing the westward geostrophic flow around

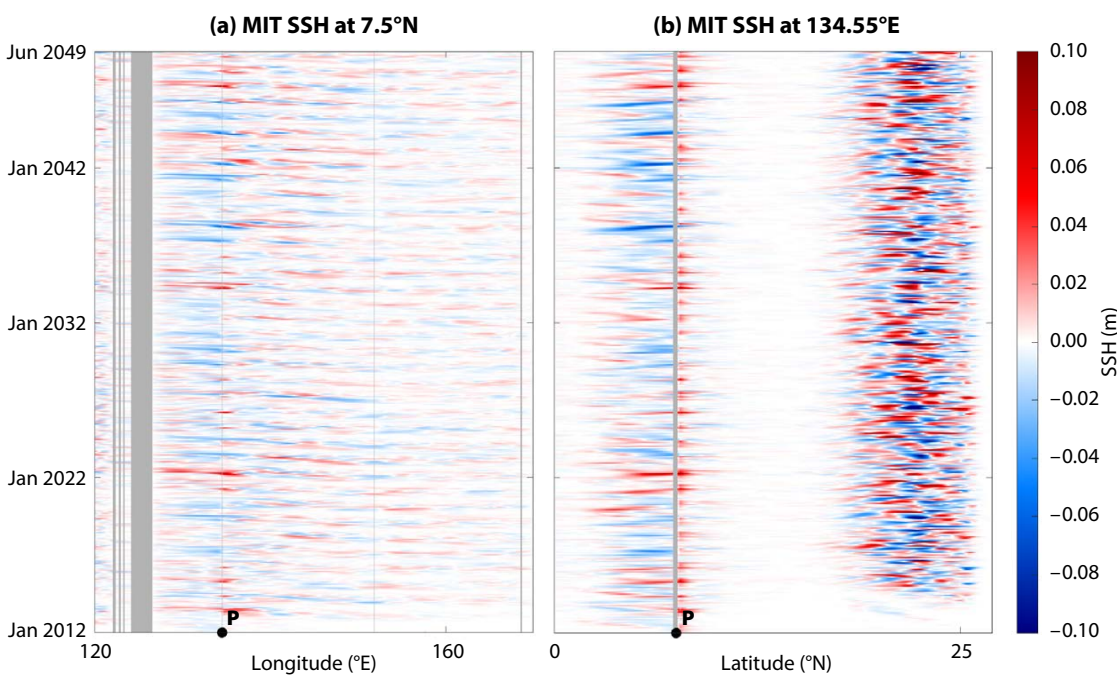


**FIGURE 3.** Hovmöller plot for SSH differences (NoP-CTL) from the 37-year-long climatological simulations. Panel (a) shows a section along latitude 7.5°N from 120°E to 170°E, and the panel (b) shows a section along longitude 134.55°E from 0°N to 27°N, both centered on Palau. The vertical gray lines mark the land, and the shading indicates SSH differences in m. The location of Palau (P) is shown on the x-axes.

the north while slowing it in front of and behind the island. Island wakes may also contribute to this signal, although they are not resolved with this model resolution. The SSH differences show similar flow deflection to the south but are not significant due to the strong NECC variability and perhaps the northeast-southwest topographic orientation.

Figure 4b,c shows the mean velocity differences (NoP-CTL) at the surface and at 1,200 m depth. At the surface, Palau obstructs the westward-flowing NEC, producing anticyclonic (cyclonic) circulation at the northern (southern) edges of the island, while slowing the westward flow to the east and west. The magnitudes of the mean velocity differences are  $\sim 5 \text{ cm s}^{-1}$  at the surface and  $\sim 1 \text{ cm s}^{-1}$  at 1,200 m depth, about 25% and 10% of the flow variability near Palau at the surface and at 1,200 m, respectively. At 1,200 m, the NEUC (Qiu et al., 2013) flows east-

ward near Palau, and the mean velocity difference pattern is reverse that of the surface. The island in CTL blocks the eastward flow, which shows a positive difference in (NoP-CTL) west of Palau. At the northern and southern edges of Palau, the eastward flow is stronger for CTL than NoP, resulting in negative zonal velocity differences and cyclonic (anticyclonic) circulation at the northern (southern) edges of Palau. The upstream influence of the island is different at the two depths. The upstream influence at 1,200 m depth extends nearly 800 km to the Philippine coast, compared to only about 100 km upstream to the east at the surface. This is hypothesized to be a consequence of the westward propagation of planetary waves that extend to the islands to the west but not to the east.

The mean vertical velocity differences at 1,200 m depth are  $\pm 10 \text{ cm day}^{-1}$ , about 10% of the vertical velocity variability

near Palau (Figure 4d). Downwelling (upwelling) features are seen at the northern (southern) end of Palau, and a downwelling feature extends from the southern edge of Palau toward the Philippine coast, which may be due to the interaction of the NEUC jet with eastward flowing zonal deep flow south of Palau, perhaps related to the NECC.

Figure 5 shows vertical zonal and meridional sections of CTL and (NoP-CTL). The latitude-depth section of mean zonal velocity (Figure 5a) averaged over the longitude range  $130^{\circ}\text{E}$ – $135^{\circ}\text{E}$ , plotted along  $0^{\circ}\text{N}$ – $27^{\circ}\text{N}$  for CTL, shows strong near-surface NEC and NECC. The NEC extends to a depth of about 300 m, whereas the NECC extends deeper, to about 500 m off the equator, but connects to deep eastward flow on the equator, as shown in previous work (Figure 1b of Qiu et al., 2013). The NEUC jets in this unconstrained climatological simulation

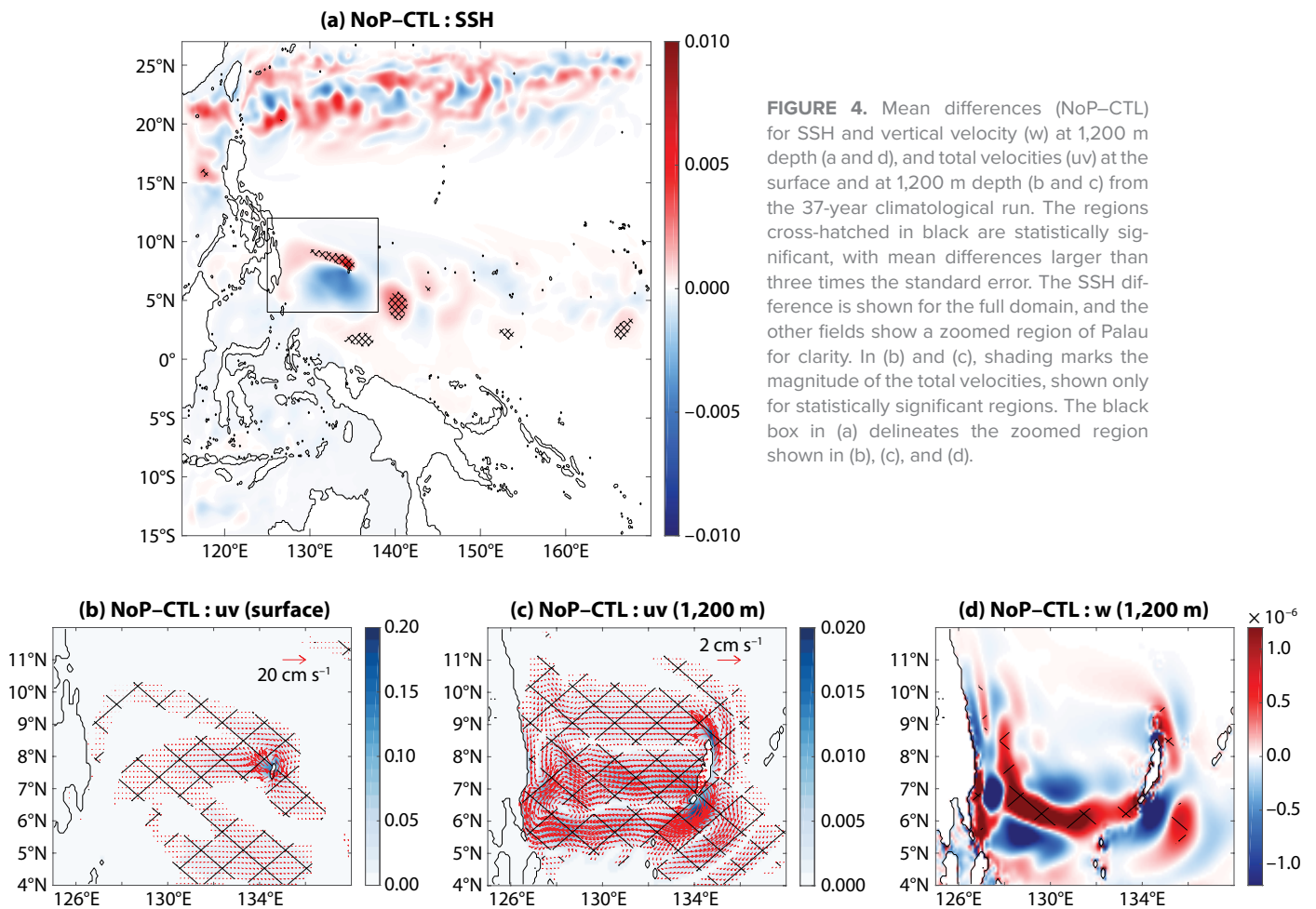


**FIGURE 4.** Mean differences (NoP-CTL) for SSH and vertical velocity ( $w$ ) at 1,200 m depth (a and d), and total velocities ( $uv$ ) at the surface and at 1,200 m depth (b and c) from the 37-year climatological run. The regions cross-hatched in black are statistically significant, with mean differences larger than three times the standard error. The SSH difference is shown for the full domain, and the other fields show a zoomed region of Palau for clarity. In (b) and (c), shading marks the magnitude of the total velocities, shown only for statistically significant regions. The black box in (a) delineates the zoomed region shown in (b), (c), and (d).

are weaker than observed (Figure 2a of Qiu et al., 2013), and undercurrent cores located at 9°N, 13°N, and 18°N are slightly offset to the north. The mean zonal velocity at Palau is eastward at depths greater than 300 m and westward near the surface (0–300 m).

The latitude-depth section of (NoP–CTL) mean zonal velocity difference (Figure 5d) at Palau shows two-layered, oppositely directed flows deflected by the island. The longitude-depth sections (along 130°E–140°E) of meridional velocity differences (NoP–CTL) at the north (8°N) and south (7°N) ends of Palau also show the two-layered flow (Figure 5b,e). The velocity difference patterns near Palau reverse between the surface and deep layers and at the northern and southern ends. This reversal of the meridional velocity difference patterns is due to the oppositely directed surface-flowing NEC and NEUC deep jets diverting around Palau.

The latitude-depth section of vertical velocity averaged over 130°E–135°E, plotted along 0°N–10°N for the CTL case (Figure 5c), shows complicated structure with strong surface downwelling south of Palau near the NECC region.

CTL also shows weak upwelling between 500 m and 1,000 m depth south of Palau, and downwelling extending throughout the water column at the southern edge of Palau. The presence of Palau results in downwelling (upwelling) at the northern (southern) edge, extending throughout the water column. These features are presumably strongly affected south of Palau by the NECC and NEUC jets.

### Modifications to the Topographic Form Stress

This study perturbed the bathymetry around Palau while keeping the same atmospheric forcing, open-ocean boundary conditions, and initial conditions. Changes to the bathymetry can affect topographic form stress (TFS), as seen in the differences between the CTL and NoP simulations. The mean zonal momentum balance should be between atmospheric wind forcing and bottom form stress across submarine ridges, seamounts, and land masses (Munk and Palmén, 1951), although boundary conditions play a role because the present model domain does not cover the whole Pacific Ocean. Following the methodology described in Masich et al. (2015)

and Wang et al. (2016), zonal TFS is computed as the pressure difference between the eastern and western face of a topographic feature divided by the width of the feature; thus, it is assumed to be uniformly distributed within the feature. The TFS represents the momentum transfer from the ocean into the land masses, acting to dissipate the ocean momentum, which is primarily fed by atmospheric winds. TFS is strongly variable in depth and time, making it difficult to interpret, and it is normally vertically integrated to a smoother field that represents total bottom form stress. Figure 6 shows the vertically integrated TFS from 0 m to 300 m depth and from 300 m to 3,000 m depth for CTL and (NoP–CTL) cases. For CTL, 0–300 m, the TFS is mainly concentrated in the Philippines, Papua, and Papua New Guinea, with values in the range  $\pm 1 \text{ N m}^{-2}$ . The TFS at Palau is positive, with values of the order of  $0.1 \text{ N m}^{-2}$  (shown in the inset in Figure 6a). Because Palau blocks the near-surface, westward-flowing NEC, the pressure gradient (east-west) is positive and results in a total positive vertically integrated TFS. The Sulu Sea forms a small enclosed water body that exhib-

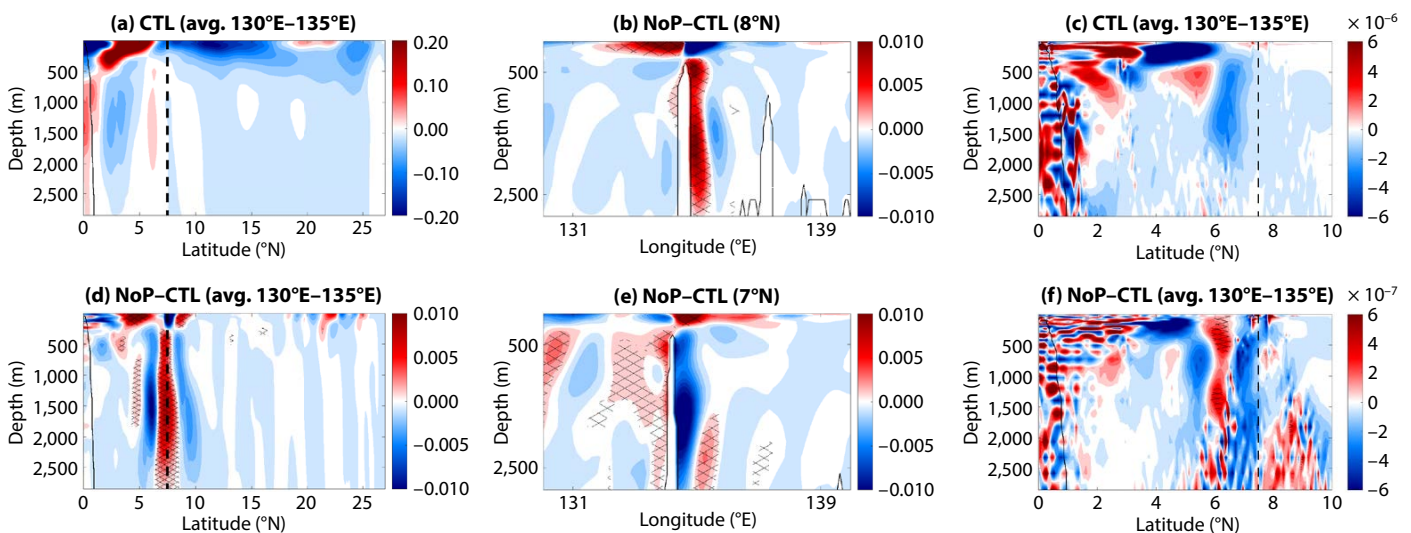


**FIGURE 5.** Vertical sections for zonal, meridional, and vertical velocity. The left column panels (a and d) show mean zonal velocity (averaged over 130°E–135°E) along 0°N–27°N for CTL (a) and for mean zonal velocity differences (NoP–CTL) (d). The middle column panels (b and e) show mean differences (NoP–CTL) of meridional velocity along 130°E–140°E at 8°N (b) and 7°N (e). The right column panels (c and f) show mean vertical velocity (averaged over 130°E–135°E) along 0°N–10°N for CTL (c) and for mean vertical velocity differences (NoP–CTL) (f). The model solutions are from the 37-year climatological run. The black cross-hatching indicates areas with statistically significant differences with the mean difference larger than three times the standard error. The vertical black dashed lines in (a), (c), (d), and (f) mark the location of Palau.

its low pressure and less dense water with increasing depth (from 200 m to 4,000 m) when compared to the water masses on its eastern, Philippine and western, Indonesian coastal boundaries. This results in a canceling positive (east) and negative (west) vertically integrated TFS across the region that encloses the Sulu Sea. For the (NoP-CTL) case, the TFS differences are focused at Palau with negative values of about  $0.1 \text{ N m}^{-2}$ . This suggests that Palau contributes  $<10\%$  of the total local TFS distribution.

For the CTL case, vertically integrated TFS (300 m to 3,000 m) follows a similar pattern as that for 0–300 m, with val-

ues in the range  $\pm 6 \text{ N m}^{-2}$ . The TFS at Palau is negative with values of the order of  $0.1 \text{ N m}^{-2}$ . At depth, the zonal flow is directed eastward and causes a negative pressure gradient (east-west). The (NoP-CTL) case TFS differences are significant at Palau as well as along the Philippines south of Palau. The TFS differences at Palau are positive with values of about  $0.1 \text{ N m}^{-2}$ . Overall, the effect of Palau on the distribution of the total TFS is not significant, and the stress redistributes locally within the region when the island is not present.

Looking at the vertical vorticity balance instead of the momentum balance

can be simpler when potential vorticity is nearly conserved. The topography enters the vorticity equation through the joint effect of baroclinicity and relief (JEBAR; Sarkisyan and Ivanov, 1971) in the vertically integrated vorticity equation. We have concentrated on the momentum equations because the complicated and abrupt topography violates the quasi-geostrophic assumption, as is evident in the presence of form stress, and the curl terms cannot be calculated as close to the island as the momentum terms because of the extra derivative in the formulations. Likewise, the presence of the form stress shows that the island rule (Godfrey, 1989;

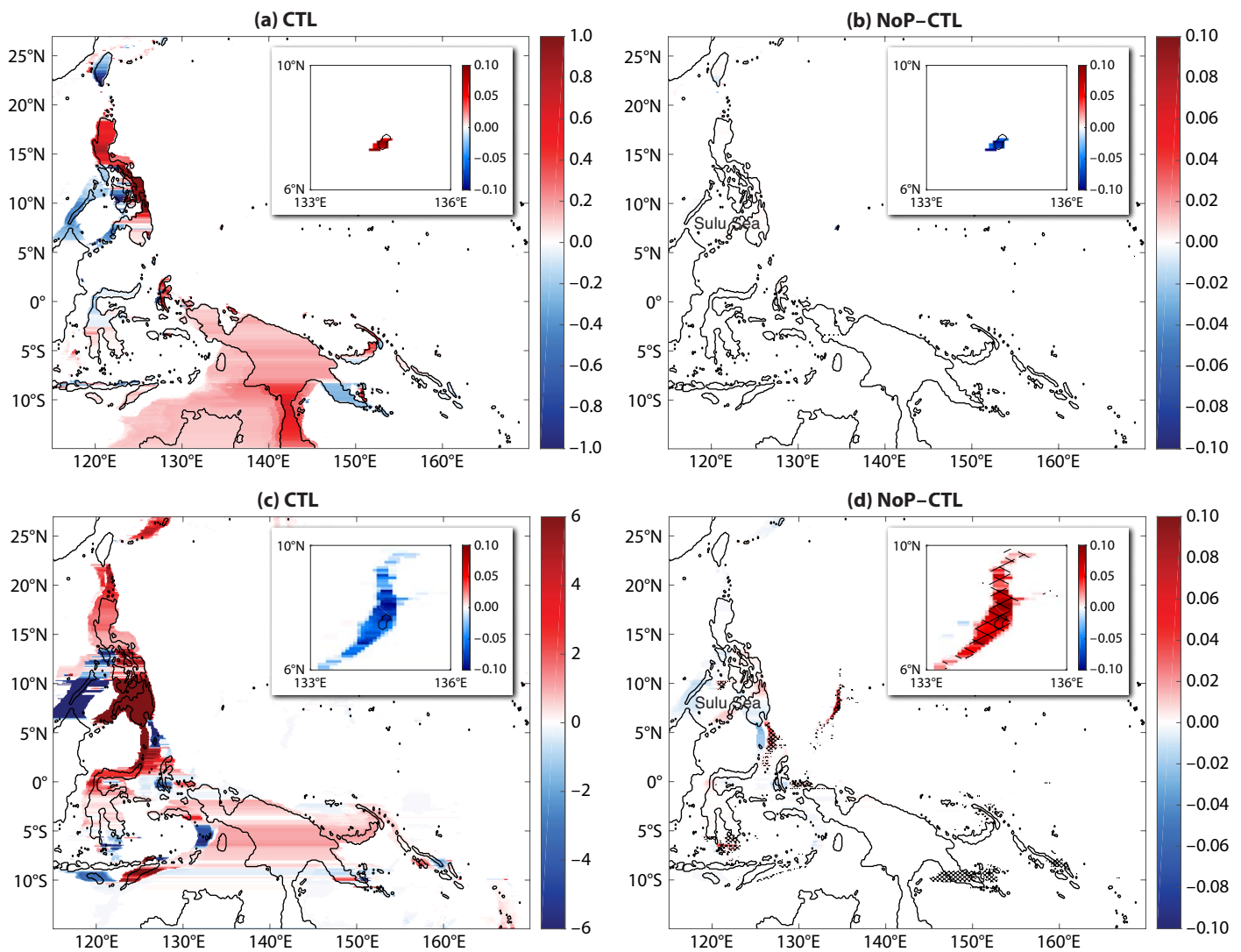


**FIGURE 6.** Topographic form stress (TFS) distribution. The top panels show vertically integrated (0–300 m) TFS distribution for the CTL (left panel) and the (NoP-CTL) (right panel). The bottom panels are the same as the top panels, but for TFS integrated from 300 m to 3,000 m. The inset plots in each subplot show the zoomed TFS distribution for Palau, for CTL, and for (NoP-CTL). The region cross-hatched in black shows statistically significant differences with the mean difference larger than three times the standard error.




Wajsowicz, 1993), which assumes a constant streamfunction around the island, is slightly violated around Palau.

## SUMMARY AND CONCLUSIONS

A regional implementation of the MITgcm for the northwestern tropical Pacific is used to understand the effect of Palau on the large-scale regional ocean circulation. Two 37-year OGCM simulations were performed with identical setups except for topography (with and without Palau). Both simulations were initialized using the same HYCOM/NCODA initial conditions and were forced using monthly climatological HYCOM/NCODA open-ocean boundary conditions, ERA-Interim atmospheric fields, and runoff fluxes.

The effects of Palau on the circulation are small, and only significantly above the eddy noise in a few places. The SSH differences are about 20% of the long-term SSH variability near Palau, and it takes about two years for the effects of the changes near Palau to reach higher latitudes. The model state differences for surface velocities are about 25% and are <1% for surface temperature and salinity, expressed as percentage of model variability near Palau from the long-term solution. The subsurface velocity differences had the same two-layer structure as the mean unperturbed flows, the westward-flowing, near-surface NEC and the eastward-flowing, subsurface NEUC jets. The surface flow patterns at the northern edge of Palau were influenced by the NEC, whereas the NECC affects the circulation at the southern edge of Palau. The zonal and meridional velocity differences showed small-scale geostrophic flow modifications around Palau but exhibited only small effect on the flows simulated using the model with horizontal grid spacing of ~9 km (Table 1). The effect of Palau on the time-mean vertically integrated TFS is significant only in a few places and is <10% of the unperturbed mean total TFS in the 5°N–10°N latitudinal band.

A caveat for this study is that it does not fully resolve the fine-scale circulation fea-

tures around Palau, such as island wakes with lee waves and eddies. These features would likely increase the form drag, so the results here are a lower bound on the effects of the islands. Likewise, the effects of the island on mixing will not be apparent in these simulations. The results are limited by model resolution and physics and are only used to explore the impact of Palau on the larger-scale regional circulation, as a complement to high-resolution modeling studies and observations focusing on the fine-scale flow modifications around Palau, some of which appear in this special issue. 

## REFERENCES

- Chassignet, E., H. Hurlburt, O. Smedstad, G. Halliwell, P. Hogan, A. Wallcraft, R. Baraille, and R. Bleck. 2007. The HYCOM (HYbrid Coordinate Ocean Model) data assimilative system. *Journal of Marine Systems* 65(1–4):60–83, <https://doi.org/10.1016/j.jmarsys.2005.09.016>.
- Cummings, J.A. 2005. Operational multivariate ocean data assimilation. *Quarterly Journal of the Royal Meteorological Society* 131(613):3,583–3,604, <https://doi.org/10.1256/qj.05.105>.
- Dee, D.P., S.M. Uppala, A.J. Simmons, P. Berrisford, P. Poli, S. Kobayashi, U. Andrae, M.A. Balmaseda, G. Balsamo, P. Bauer, and others. 2011. The ERA-Interim reanalysis: Configuration and performance of the data assimilation system. *Quarterly Journal of the Royal Meteorological Society* 137(656):553–597, <https://doi.org/10.1002/qj.828>.
- Ducet, N., P.-Y. Le Traon, and G. Reverdin. 2000. Global high-resolution mapping of ocean circulation from TOPEX/Poseidon and ERS-1 and -2. *Journal of Geophysical Research* 105(C8):19,477–19,498, <https://doi.org/10.1029/2000JC900063>.
- Edwards, C., T. Fake, and P. Bogden. 2004a. Spring-summer frontogenesis at the mouth of Block Island Sound: Part 1. A numerical investigation into tidal and buoyancy-forced motion. *Journal of Geophysical Research* 109(C12), <https://doi.org/10.1029/2003JC002132>.
- Edwards, C., T. Fake, D. Codiga, and P. Bogden. 2004b. Spring-summer frontogenesis at the mouth of Block Island Sound: Part 2. Combining acoustic Doppler current profiler records with a general circulation model to investigate the impact of subtidal forcing. *Journal of Geophysical Research* 109(C12), <https://doi.org/10.1029/2003JC002133>.
- Fekete, B.M., C.J. Vörösmarty, and W. Grabs. 2002. High-resolution fields of global runoff combining observed river discharge and simulated water balances. *Global Biogeochemical Cycles* 16(3):15–1–15–10, <https://doi.org/10.1029/1999GB001254>.
- Fukumori, I., T. Lee, B. Cheng, and D. Menemenlis. 2004. The origin, pathway, and destination of Niño-3 water estimated by a simulated passive tracer and its adjoint. *Journal of Physical Oceanography* 34:582–604, <https://doi.org/10.1175/2515.1>.
- Godfrey, J. 1989. A Sverdrup model of the depth-integrated flow for the world ocean allowing for island circulations. *Geophysical & Astrophysical Fluid Dynamics* 45(1–2):89–112, <https://doi.org/10.1080/03091928908208894>.
- Gopalakrishnan, G., B.D. Cornuelle, and I. Hoteit. 2013a. Adjoint sensitivity studies of loop current and eddy shedding in the Gulf of Mexico. *Journal of Geophysical Research* 118(7):3,315–3,335, <https://doi.org/10.1002/jgrc.20240>.
- Gopalakrishnan, G., B.D. Cornuelle, I. Hoteit, D.L. Rudnick, and W.B. Owens. 2013b. State estimates and forecasts of the Loop Current in the Gulf of Mexico using the MITgcm and its adjoint. *Journal of Geophysical Research* 118(7):3,292–3,314, <https://doi.org/10.1002/jgrc.20239>.
- Gopalakrishnan, G., B.D. Cornuelle, G. Gawarkiewicz, and J.L. McClean. 2013c. Structure and evolution of the cold dome off northeastern Taiwan: A numerical study. *Oceanography* 26(1):66–79, <https://doi.org/10.5670/oceanog.2013.06>.
- Hoteit, I., B. Cornuelle, S.Y. Kim, G. Forget, A. Kohl, and E. Terrill. 2009. Assessing 4D-VAR for dynamical mapping of coastal high-frequency radar in San Diego. *Dynamics of Atmospheres and Oceans* 48(1–3):175–197, <https://doi.org/10.1016/j.dynatmoce.2008.11.005>.
- Hoteit, I., B. Cornuelle, and P. Heimbach. 2010. An eddy-permitting, dynamically consistent adjoint-based assimilation system for the tropical Pacific: Hindcast experiments in 2000. *Journal of Geophysical Research* 115(C3), <https://doi.org/10.1029/2009JC005437>.
- Karnauskas, K.B., R. Murtugudde, and A.J. Busalacchi. 2007. The effect of the Galápagos Islands on the equatorial Pacific cold tongue. *Journal of Physical Oceanography* 37(5):1,266–1,281, <https://doi.org/10.1175/JPO3048.1>.
- Kashino, Y., A. Ishida, and S. Hosoda. 2011. Observed ocean variability in the Mindanao Dome region. *Journal of Physical Oceanography* 41(2):287–302, <https://doi.org/10.1175/2010JPO4329.1>.
- Kashino, Y., A. Atmadipoera, and Y. Kuroda. 2013. Observed features of the Halmahera and Mindanao eddies. *Journal of Geophysical Research* 118(12):6,543–6,560, <https://doi.org/10.1002/2013JC009207>.
- Kim, S.Y., G. Gopalakrishnan, and A. Ponte. 2015. Interpretation of coastal wind transfer functions with momentum balances derived from idealized numerical model simulations. *Ocean Dynamics* 65(1):115–141, <https://doi.org/10.1007/s10236-014-0766-x>.
- Kohl, A., D. Stammer, and B. Cornuelle. 2007. Interannual to decadal changes in the ECCO global synthesis. *Journal of Physical Oceanography* 37(2):313–337, <https://doi.org/10.1175/JPO3014.1>.
- Large, W., and S. Pond. 1981. Open ocean momentum flux measurements in moderate to strong winds. *Journal of Physical Oceanography* 11(3):324–336, [https://doi.org/10.1175/1520-0485\(1981\)011<0324:OOMFMI>2.0.CO;2](https://doi.org/10.1175/1520-0485(1981)011<0324:OOMFMI>2.0.CO;2).
- Large, W.G., J.C. McWilliams, and S.C. Doney. 1994. Oceanic vertical mixing: A review and a model with a nonlocal boundary layer parameterization. *Reviews of Geophysics* 32(4):363–403, <https://doi.org/10.1029/94RG01872>.
- Legg, S., R. Hallberg, and J. Girton. 2006. Comparison of entrainment in overflows simulated by z-coordinate, isopycnal and non-hydrostatic models. *Ocean Modelling* 11:69–97, <https://doi.org/10.1016/j.ocemod.2004.11.006>.
- Lien, R.-C., B. Ma, C.M. Lee, T.B. Sanford, V. Mensah, L.R. Centurioni, B.D. Cornuelle, G. Gopalakrishnan, A.L. Gordon, M.-H. Chang, and others. 2015. The Kuroshio and Luzon Undercurrent east of Luzon Island. *Oceanography* 28(4):54–63, <https://doi.org/10.5670/oceanog.2015.81>.

- Marshall, J., A. Adcroft, C. Hill, L. Perelman, and C. Heisey. 1997. A finite-volume, incompressible Navier Stokes model for studies of the ocean on parallel computers. *Journal of Geophysical Research* 102(C3):5,753–5,766, <https://doi.org/10.1029/96JC02775>.
- Masich, J., T.K. Chereskin, and M.R. Mazloff. 2015. Topographic form stress in the Southern Ocean state estimate. *Journal of Geophysical Research* 120(12):7,919–7,933, <https://doi.org/10.1002/2015JC011143>.
- Masumoto, Y., and T. Yamagata. 1991. Response of the western tropical Pacific to the Asian winter monsoon: The generation of the Mindanao Dome. *Journal of Physical Oceanography* 21(9):1,386–1,398, [https://doi.org/10.1175/1520-0485\(1991\)021<1386:ROTWTP>2.0.CO;2](https://doi.org/10.1175/1520-0485(1991)021<1386:ROTWTP>2.0.CO;2).
- Mazloff, M., P. Heimbach, and C. Wunsch. 2010. An eddy-permitting Southern Ocean state estimate. *Journal of Physical Oceanography* 40:880–899, <https://doi.org/10.1175/2009JPO4236.1>.
- Menemenlis, D., I. Fukumori, and T. Lee. 2005. Using Green's functions to calibrate an ocean general circulation model. *Monthly Weather Review* 133(5):1,224–1,240, <https://doi.org/10.1175/MWR2912.1>.
- Munk, W.H., and E. Palmén. 1951. Note on the dynamics of the Antarctic Circumpolar Current. *Tellus* 3(1):53–55, <https://doi.org/10.3402/tellusa.v3i1.8609>.
- Musgrave, R., and T. Peacock. 2016. The momentum balance of steady flow past an island. Paper presented at the VIII<sup>th</sup> International Symposium on Stratified Flows, August 29–September 1, 2016, San Diego, California.
- Nitani, H. 1972. Beginning of the Kuroshio. Pp. 129–163 in *Kuroshio, its Physical Aspects*. H. Stommel and K. Yoshida, eds, University of Tokyo Press.
- Qiu, B. 1999. Seasonal eddy field modulation of the North Pacific Subtropical Countercurrent: TOPEX/Poseidon observations and theory. *Journal of Physical Oceanography* 29(10):2,471–2,486, [https://doi.org/10.1175/1520-0485\(1999\)029<2471:SEFMOT>2.0.CO;2](https://doi.org/10.1175/1520-0485(1999)029<2471:SEFMOT>2.0.CO;2).
- Qiu, B., and S. Chen. 2010. Interannual variability of the North Pacific Subtropical Countercurrent and its associated mesoscale eddy field. *Journal of Physical Oceanography* 40(1):213–225, <https://doi.org/10.1175/2009JPO4285.1>.
- Qiu, B., D.L. Rudnick, S. Chen, and Y. Kashino. 2013. Quasi-stationary North Equatorial Undercurrent jets across the tropical North Pacific Ocean. *Geophysical Research Letters* 40(10):2,183–2,187, <https://doi.org/10.1002/grl.50394>.
- Qiu, B., D.L. Rudnick, I. Cerovecki, B.D. Cornuelle, S. Chen, M.C. Schönau, J.L. McClean, and G. Gopalakrishnan. 2015. The Pacific North Equatorial Current: New insights from the Origins of the Kuroshio and Mindanao Currents (OKMC) Project. *Oceanography* 28:24–33, <https://doi.org/10.5670/oceanog.2015.78>.
- Qu, T., H. Mitsudera, and T. Yamagata. 1998. On the western boundary currents in the Philippine Sea. *Journal of Geophysical Research* 103(C4):7,537–7,548, <https://doi.org/10.1029/98JC00263>.
- Qu, T., and R. Lukas. 2003. The bifurcation of the North Equatorial Current in the Pacific. *Journal of Physical Oceanography* 33(1):5–18, [https://doi.org/10.1175/1520-0485\(2003\)033<0005:TBOTNE>2.0.CO;2](https://doi.org/10.1175/1520-0485(2003)033<0005:TBOTNE>2.0.CO;2).
- Sarkisyan, A., and V. Ivanov. 1971. The combined effect of baroclinicity and bottom relief as an important factor in the dynamics of ocean currents. (AGU translation) *Izvestiya, Academy of Sciences, USSR, Atmospheric and Oceanic Physics* 2:173–188.
- Schönau, M.C., D.L. Rudnick, I. Cerovecki, G. Gopalakrishnan, B.D. Cornuelle, J.L. McClean, and B. Qiu. 2015. The Mindanao Current: Mean structure and connectivity. *Oceanography* 28(4):34–45, <https://doi.org/10.5670/oceanog.2015.79>.
- Schönau, M.C., and D.L. Rudnick. 2017. Mindanao Current and Undercurrent: Thermohaline structure and transport from repeat glider observations. *Journal of Physical Oceanography* 47(8):2,055–2,075, <https://doi.org/10.1175/JPO-D-16-0274.1>.
- Schönau, M.C., H.W. Wijesekera, W.J. Teague, P.L. Colin, G. Gopalakrishnan, D.L. Rudnick, B.D. Cornuelle, Z.R. Hallock, and D.W. Wang. 2019. The end of an El Niño: A view from Palau. *Oceanography* 32(4):32–45, <https://doi.org/10.5670/oceanog.2019.409>.
- Schramek, T.A., B.D. Cornuelle, G. Gopalakrishnan, P.L. Colin, S.J. Rowley, M.A. Merrifield, and E.J. Terrill. 2019. Tropical western Pacific thermal structure and its relationship to ocean surface variables: A numerical state estimate and forereef temperature records. *Oceanography* 32(4):156–163, <https://doi.org/10.5670/oceanog.2019.421>.
- Stammer, D., C. Wunsch, R. Giering, C. Eckert, P. Heimbach, J. Marotzke, A. Adcroft, C. Hill, and J. Marshall. 2002. Global ocean circulation during 1992–1997, estimated from ocean observations and a general circulation model. *Journal of Geophysical Research* 107(C9), 1–1–1-27, <https://doi.org/10.1029/2001JC000888>.
- Wajswicz, R.C. 1993. The circulation of the depth-integrated flow around an island with application to the Indonesian throughflow. *Journal of Physical Oceanography* 23(7):1,470–1,484, [https://doi.org/10.1175/1520-0485\(1993\)023<1470:TCOTDI>2.0.CO;2](https://doi.org/10.1175/1520-0485(1993)023<1470:TCOTDI>2.0.CO;2).
- Wang, J., M.R. Mazloff, and S.T. Gille. 2016. The effect of the Kerguelen Plateau on the ocean circulation. *Journal of Physical Oceanography* 46(11):3,385–3,396, <https://doi.org/10.1175/JPO-D-15-0216.1>.
- Zhang, X., B. Cornuelle, and D. Roemmich. 2012. Sensitivity of western boundary transport at the mean North Equatorial Current bifurcation latitude to wind forcing. *Journal of Physical Oceanography* 42:2,056–2,072, <https://doi.org/10.1175/JPO-D-11-0229.1>.

## ACKNOWLEDGMENTS

The MITgcm code used in this study is checkpoint 64Y, obtained from [http://mitgcm.org/public/source\\_code.html](http://mitgcm.org/public/source_code.html). The SSALTO/DUACS altimeter product AVISO is produced and distributed by the Copernicus Marine and Environment Monitoring Service (CMEMS; <http://marine.copernicus.eu/>). The HYCOM/NCODA 1/12° global analysis data were obtained from the HYCOM consortium (<http://hycom.org/dataserver/>). The ERA-Interim atmospheric forcings were obtained from the ECMWF (<https://www.ecmwf.int/en/forecasts/datasets/reanalysis-datasets/era-interim>). We gratefully acknowledge support from the Office of Naval Research Departmental Research Initiative: Flow Encountering Abrupt Topography (FLEAT).

## AUTHORS

**Ganesh Gopalakrishnan** (ggopalakrishnan@ucsd.edu) is Project Scientist, and **Bruce D. Cornuelle** is Researcher, both in the Department of Climate, Atmospheric Science, and Physical Oceanography, Scripps Institution of Oceanography, University of California San Diego, La Jolla, CA, USA.

## ARTICLE CITATION

Gopalakrishnan, G., and B.D. Cornuelle. 2019. Palau's effects on regional-scale ocean circulation. *Oceanography* 32(4):126–135, <https://doi.org/10.5670/oceanog.2019.418>.

## COPYRIGHT & USAGE

This is an open access article made available under the terms of the Creative Commons Attribution 4.0 International License (<https://creativecommons.org/licenses/by/4.0/>), which permits use, sharing, adaptation, distribution, and reproduction in any medium or format as long as users cite the materials appropriately, provide a link to the Creative Commons license, and indicate the changes that were made to the original content.